



An investigation on corrosion protection layers in pipelines transporting hydrocarbons

Gabriella Bolzon

Politecnico di Milano, Department of Civil and Environmental Engineering
gabriella.bolzon@polimi.it

Giovanna Gabetta

eni E&P Division
giovanna.gabetta@eni.com

Bernardo Molinas

Venezia Tecnologie S.p.A.
bmolinas@veneziatecnologie.it

ABSTRACT. Chemical reactions between carbon steel, water and chemical species produce corrosion layers (scales) on the internal surface of pipelines transporting hydrocarbons. Scales act as a diffusion barrier and prevent the progress of corrosion, a dangerous failure initiator. The protective film (10-100 μm thickness) can be removed locally by the action of the internal flow, or by other mechanisms. Adhesion with the substrate and the failure modes of the corrosion layer can be tested by indentation. Some results are presented of experiments performed on specimens with scales grown in a controlled environment.

KEYWORDS. Pipelines; Failure; Corrosion; Protection layers; Iron carbonate scales.

INTRODUCTION

Corrosion is one of the main phenomena affecting the integrity of pipeline systems [1, 2]. Corrosion may be induced by the presence of carbon dioxide (CO_2) in the fluids transported with hydrocarbons. CO_2 dissolves in water and forms carbonic acid (H_2CO_3), which dissociates into hydrogen ions (H^+) and carbonic anion (CO_3^{2-}). H^+ ions remove electrons from the metal surface and ferrous ions Fe^{2+} dissolve. However, when Fe^{2+} and CO_3^{2-} exceed the solubility limit, precipitation of iron carbonate (FeCO_3) scales is initiated and a protective film progressively forms on the metal surface.

The morphology of the scales depends on both steel properties and environmental conditions. The compact carbonate scales grown on steel grade X65 (API specifications [3]) at different CO_2 pressure (1 bar and 170 bar, i.e. 100 kPa and 17 MPa) are shown by the SEM micrographs in Fig. 1: the characteristic size of the crystals is significantly different in the two cases; larger crystals are obtained at high pressure in supercritical CO_2 conditions. Scales can vary also in thickness, depending on the exposure time to the aggressive environment. The formation of double corrosion layers, clearly shown for instance in Fig. 2 (right) and Fig. 3 (left), may also occur [4].

Factors governing the scale growth process may influence the mechanical properties and the adhesion to the steel substrate of the corrosion layer [5, 6] and the possibility of ensuring further adequate protection. These characteristics can be verified by means of indentation tests, which allow identifying the failure modes and calibrating the mechanical properties of materials. The maximum force applied by commonly available instrumentation can vary in a wide range (from mN to kN) and tests can be performed at different penetration depths. The geometry of the indenter tip can also be appropriately selected. In particular, rounded conical (Rockwell [7]) and sharp pyramidal (Vickers [8]) tips can be used to obtain complementary information.

The material characteristics are reflected by the indentation curves, which correlate the displacement of the indenter tip to the exerted force. This information can be exploited to recover the microscopic or macroscopic mechanical properties of materials either in laboratory [9] or directly on components, possibly in situ [10]. Specific application of indentation techniques complemented by inverse analysis tools have been recently considered for the diagnostic analysis of pipeline systems [11], with the ultimate aim to prevent failures associated to progressive degradation phenomena, which may be assisted by the environmental conditions [12].

Methodologies suitable to identify the characteristics of coatings [13] and interfaces [14] in layered systems have been developed. Indentation curves can also reveal spall or cracking attitude depending on the ductility or the brittleness of the components [15].

The main results of an indentation study performed on the corrosion products grown on pipe steel samples are summarized in this contribution.

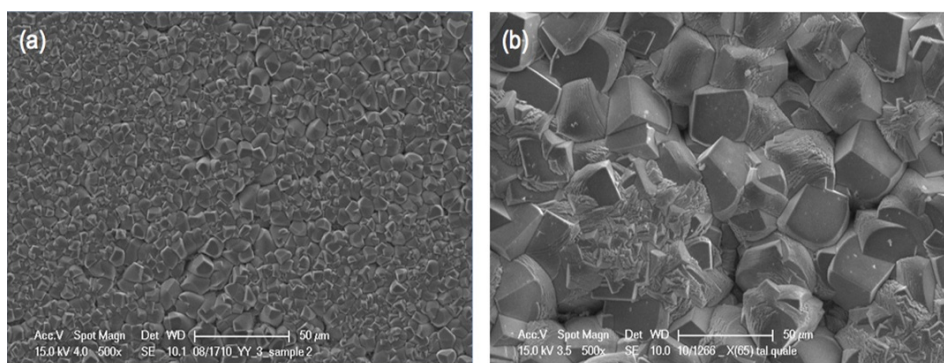


Figure 1: Morphology of carbonate scales obtained at 1 bar (a) [17] and 170 bar (b) CO₂ pressure: SEM micrographs with SE (Secondary Electrons) at the same magnification (Marker: 50 µm).

MATERIALS AND METHODS

X65 pipeline steel [3] and J55 casing steel [16] were considered. The materials have different composition and different but comparable mechanical properties, listed in Tab. 1 and Tab. 2.

Iron carbonate (FeCO₃) films were grown on polished and degreased square samples (20 × 20 mm², 3 mm thickness) inserted in Hastelloy C276 autoclave in saturated CO₂ conditions at 70°C. The substrate was exposed for 68 hours to a synthetic fluid, with composition reported in Tab. 3.

Specimens were observed with optical and electronic microscope. X ray diffraction (XRD) analysis was performed to identify scale composition. Details on specimen preparation and characterization are reported in [17] and [18].

	C	Si	Mn	P	S	Cr	Ni	Mo	Cu	Nb	Ti	Al	V	N
X65	0.048	0.21	1.40	0.0220	0.002	0.018	-	0.200	0.01	0.4	0.007	0.04	-	-
J55	0.350	0.39	0.87	0.0015	0.008	0.130	0.12	0.018	0.23	-	-	0.007	<0.01	-

Table 1: Chemical composition of the steel substrates (max %).

The mechanical response of the specimens was investigated by indentation tests, performed with rounded (Rockwell [7]) and sharp (Vickers [8]) tips at 100 N and 200 N maximum load in a Zwick/Roell ZHU 0,2 equipment. The different characteristics of the surface layers were clearly reflected by the indentation curves, shown in Fig. 4 and Fig. 5 for X65 steel substrate.

	Minimum yield limit	Maximum yield limit	Minimum tensile strength	Maximum tensile strength
X65	448 MPa (65 psi)	600 MPa (87 psi)	531 MPa (77 psi)	758 MPa (110 psi)
J55	379 MPa (55 psi)	552 MPa (80 psi)	517 MPa (75 psi)	-

Table 2: Standard yield limit and tensile strength [3, 16].

Na Cl	K Cl	CaCl ₂ .2H ₂ O	MgCl ₂ .6H ₂ O	NaHCO ₃	Na Br	Na ₂ H ₂ O
27.331	0.235	1.790	2.133	0.427	0.126	0.147

Table 3: Salt concentration (g/l) in the corrosive autoclave environment.

Deformation and damaging phenomena induced by the mechanical action were inferred by scan electron microscopy (SEM) observation of the specimen surfaces and of some cross sections, in either secondary electron (SE) or back-scattered electron (BSE) mode. The residual imprints left on the material by the indentation test were evidenced by a careful cutting and polishing of the material samples. During this preparation, specimens were protected with an aluminum foil in order to preserve the surface layers. Thickness measurements were also performed on the micrographs. BSE images of the cross sections of scales grown on X65 steel are shown in Fig. 2. A much thicker double corrosion layer can be observed in correspondence of the side marked B (right), which was exposed to the fluid, in comparison with the opposite side A, in contact with a polyethylene sheet on the autoclave bottom during the process. Corrosion is evidenced by the presence of cementite (Fe₃C) in the modified internal part of the substrate, with a clear separation line from the external carbonate crystals (see Fig. 2, right micrograph).

The BE micrographs of Fig. 3 visualize the corrosion layers produced in sample J55 in correspondence of sides named A (left, exposed to the fluid) and B (right, in contact with the autoclave bottom).

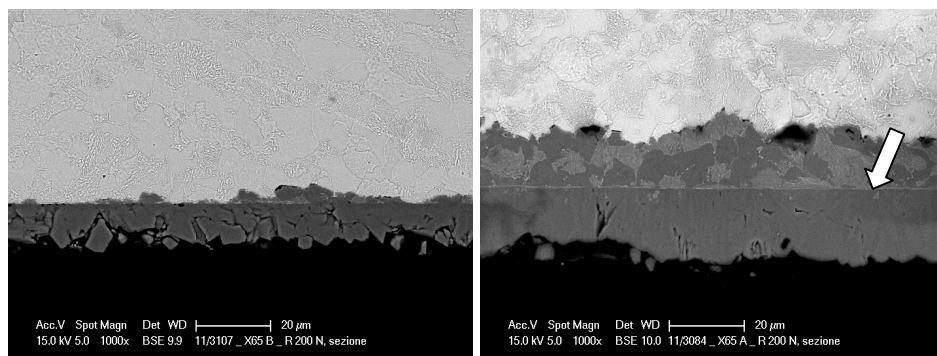


Figure 2: SEM micrographs (BSE) of the cross section of X65 corroded sample, side A in contact with the autoclave bottom (left) and side B exposed to the fluid (right) at the same magnification (Marker: 20 µm). The substrate is in the upper part of both micrographs.

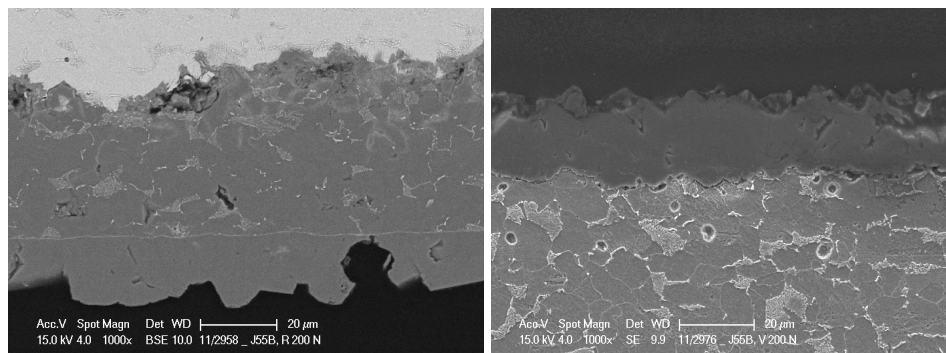


Figure 3: SEM micrographs of the cross section of J55 corroded sample, side A exposed to the fluid (left, BSE) and side B in contact with the autoclave bottom (right, SE) at the same magnification (Marker: 20 µm). The substrate is in the upper part of the micrograph (left) and in the lower part of it (right), respectively.



RESULTS AND DISCUSSION

The corroded X65 and J55 specimens were subjected to Rockwell and Vickers instrumented indentation at 100 N and 200 N maximum load. Cross sections were carefully cut through the residual imprints left on the material and were subjected to micrographic investigation, which allows to correlate the output of the mechanical tests with the damaging phenomena induced in the corrosion layers and in their substrates. A selection of results is presented and discussed in this section.

X65 steel

The indentation curves drawn in Fig. 4 and Fig. 5 were produced by Vickers and Rockwell indentation at 100 N and 200 N maximum load, respectively, on the two sides of the carbonated X65 material sample. The curves are compared with that resulting (as a mean) from tests performed on the substrate before corrosion was induced.

The graphs on the left in Fig. 4 and Fig. 5 refer to side A, in contact with the autoclave bottom. The curves are regular and conform to the output of the steel substrate, independently of the tip geometry and loading level. A systematically reduced tip penetration depth for the same applied load is observed in the case of Rockwell indentation (Fig. 5, left) while the presence of the scales is almost not detected by the Vickers test (Fig. 4, left).

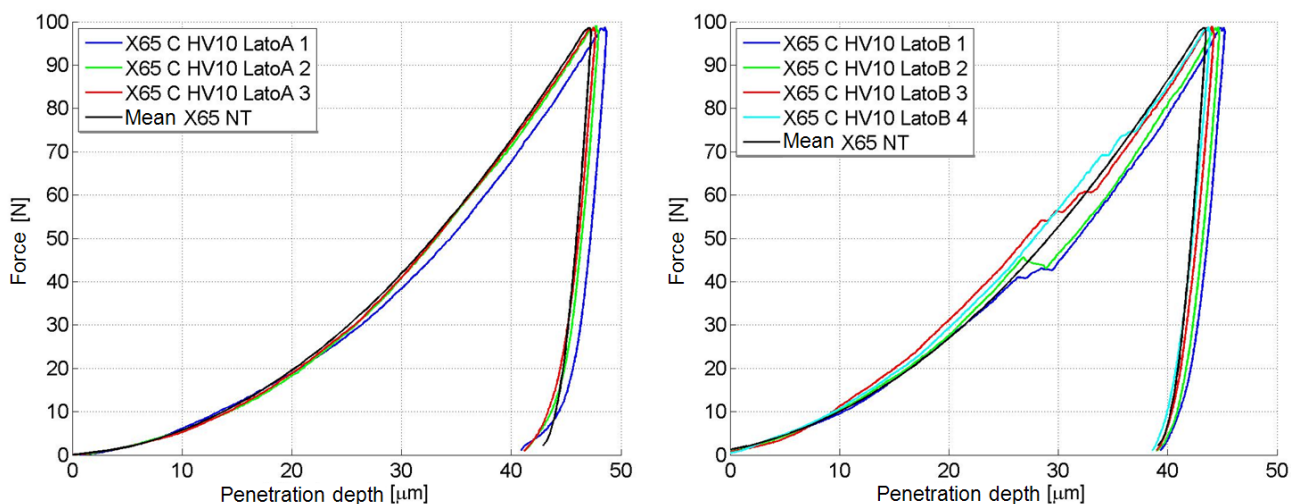


Figure 4: Indentation curves concerning X65 specimen, side A in contact with the autoclave bottom (left) and side B exposed to the fluid (right): Vickers tip at 100 N maximum load.

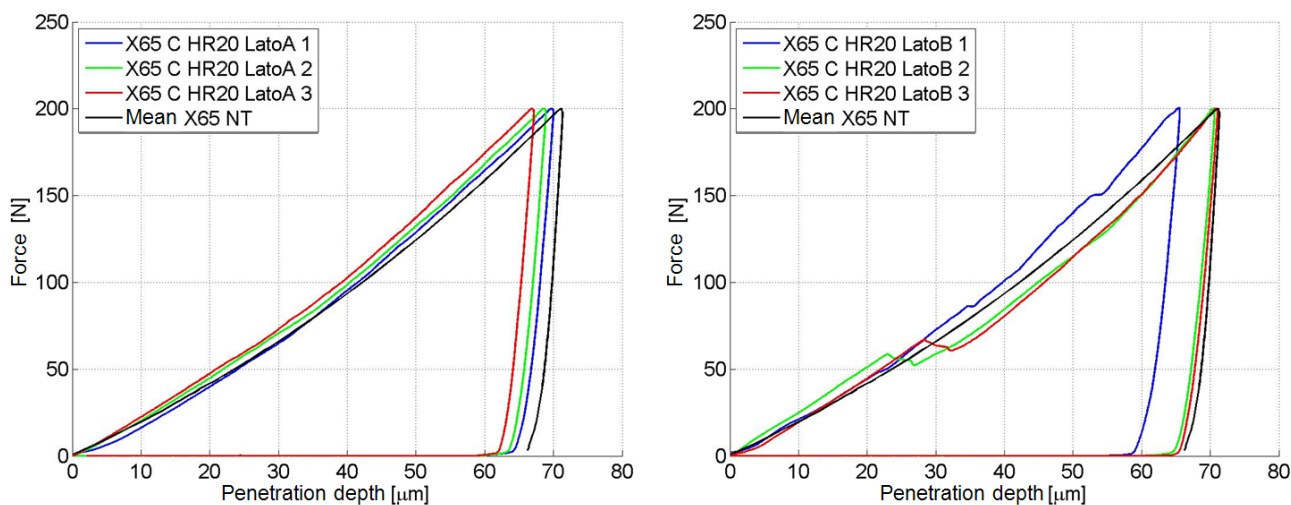


Figure 5: Indentation curves concerning X65 specimen, side A in contact with the autoclave bottom (left) and side B exposed to the fluid (right): Rockwell tip at 200 N maximum load.



Indentation provokes the detaching of scale crystals in the piling-up area of the residual imprint, evidenced by the micrographs in Fig. 6 and, in more detail, Fig. 7 and Fig. 8 (left). The effect of this phenomenon on the indentation curves is magnified by the axis-symmetric Rockwell tip although the areas of removed scales are comparable, see Fig. 6. In the region under the indenter tip, crystals are compact and no further damaging phenomena are observed.

The situation is rather different on side B, exposed to the fluid, where a thick scale coating is deposited on a corroded layer containing cementite, see Fig. 2. The corresponding indentation curves are drawn in the graphs of Fig. 4 (right) and Fig. 5 (right). The trend is typical of fracture propagation in brittle materials [15]: a series of kinks appear on the loading branch starting from about $40\div 50$ N. Cracks are clearly observed in the region underneath the wide areas of removed carbonate crystals, shown in Fig. 8 (right) and Fig. 9. The separation between the two corrosion layers is also observed, even at far distance from the imprints, see Fig. 10.

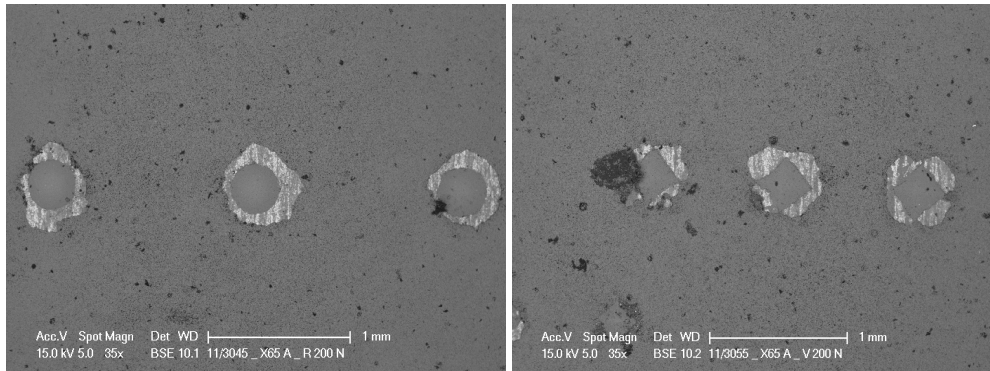


Figure 6: SEM micrograph (BSE) of the indented surface of X65 specimen, side A in contact with the autoclave bottom. Rockwell (left) and Vickers (right) tip at 200 N maximum load. Same magnification, marker: 1 mm.

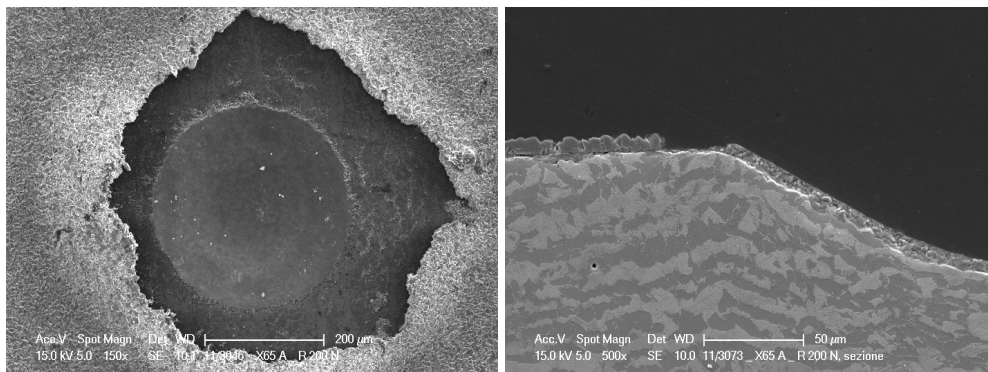


Figure 7: SEM micrograph (SE) of the specimen surface (left, marker: 200 μm) and on the cross section (right, marker 50 μm) of X65 corroded sample after Rockwell indentation at 200 N maximum load: side A, in contact with the autoclave bottom.

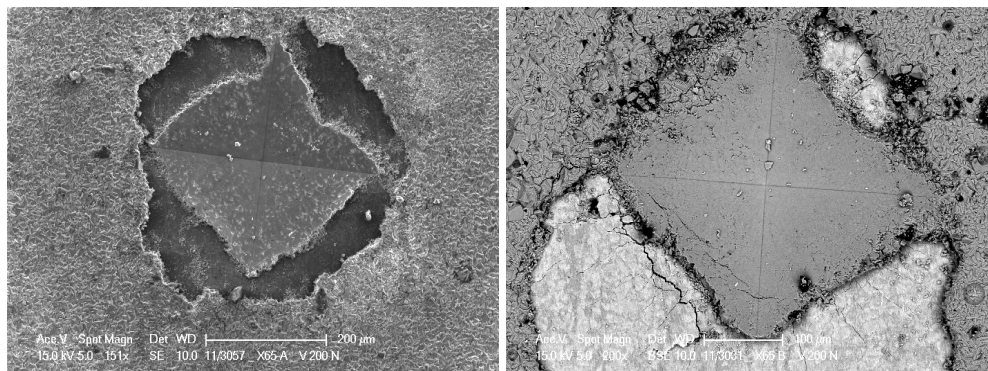


Figure 8: SEM micrographs of the specimen surface after Vickers indentation at 200 N maximum load of X65 corroded sample: side A in contact with the autoclave bottom (left, SE, marker: 200 μm) and side B exposed to the fluid (right, BSE, marker 100 μm).

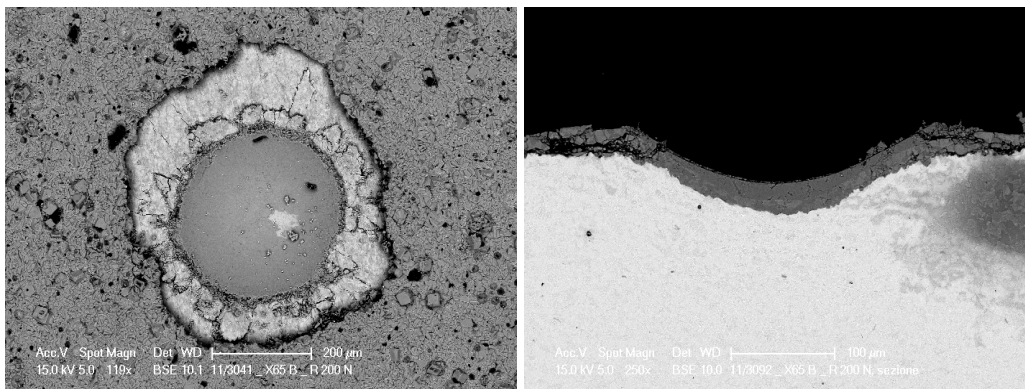
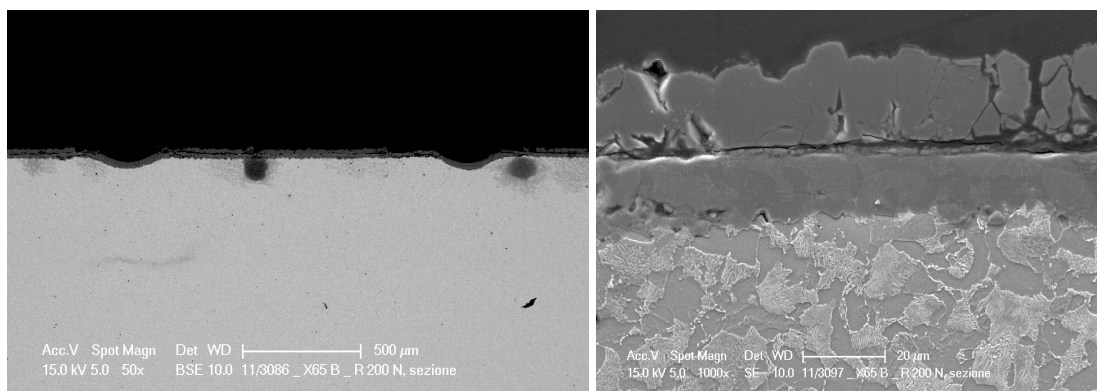


Figure 9: SEM micrograph (BSE) of the specimen surface (left, marker: 200 µm) and on the cross section (right, marker 100 µm) of X65 corroded sample after Rockwell indentation at 200 N maximum load: side B, exposed to the fluid.



F

Figure 10: SEM imaging (BSE) of the regions between two residual imprints left on side B (exposed to the fluid) of X65 corroded sample by Rockwell indentation at 200 N maximum load (left, marker: 500 µm) and a detail (SE) of the corrosion layers far from the imprints (right, marker: 20 µm). The dark spots, visible also in Fig. 9 (right), are water drops absorbed by the porous layers during the polishing of the surface and released under SEM vacuum.

J55 steel

The indentation curves relevant to Rockwell and Vickers tests performed at 200 N maximum load on the two sides of the carbonated J55 steel sample are drawn in Fig. 11 and Fig. 12. The curves are compared with the mean result of X65 substrate, as in Fig. 4 and Fig. 5.

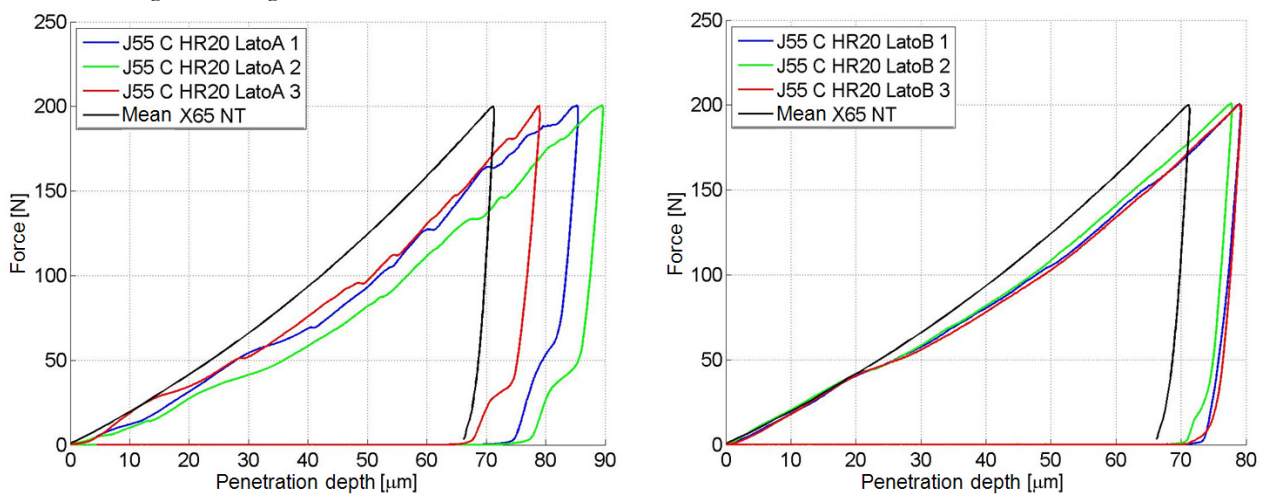


Figure 11: Indentation curves returned by Rockwell tip at 200 N maximum load on J55 specimen: side A exposed to the fluid (left) and side B in contact with the autoclave bottom (right).

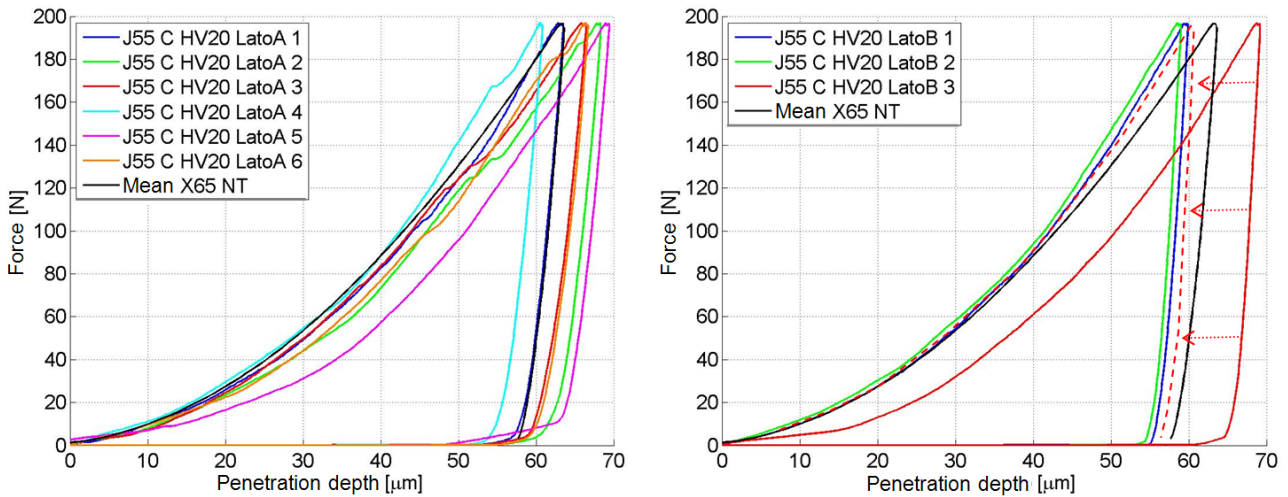


Figure 12: Indentation curves returned by Vickers tip at 200 N maximum load on J55 specimen: side A exposed to the fluid (left) and side B in contact with the autoclave bottom (right).

The specimen developed a double corrosion layer on the side (A) exposed to the fluid, an occurrence reflected again by the kinks appearing in the corresponding indentation curves, shown in Fig. 11 (left) and Fig. 12 (left). The phenomenon is particularly pronounced in the case of Rockwell indentation, see Fig. 11 (left). The unloading branch of the curves is also affected in this case, likely due to the extensive material spalling that was observed on the specimen surface after the test even by optical microscopy. On the other hand, the sample response to Vickers indentation is similar to that exhibited by X65 corroded steel, shown in Fig. 4 (right), although a larger dispersion is observed in the present case.

The curves concerning either Rockwell or Vickers indentation performed on side B (in contact with the autoclave bottom) of the corroded J55 steel sample are shown in Fig. 11 (right) and Fig. 12 (right). At the beginning, the resemblance with X65 steel response is pretty close. Then the curves deviate smoothly: more markedly and starting from about 50 N with the rounded Rockwell tip; at about 100 N for the sharp Vickers one. Notice that one curve is reported twice in Fig. 12 (right): as obtained from the equipment (continuum line) and translated (dashed) to the left as pointed out by the arrows, in order to follow the common initial trend. The fairly good overall agreement with the remaining output indicates that the initial discordance was likely due to some imperfection of the surface layer, phased out by the compression state induced by the test as the load increases, while the experimental dispersion due to the essential characteristics of the material system is quite low.

The damage profile induced by Rockwell indentation is shown in Fig. 13. The picture on the right focuses on the region of removed scales surrounding the conical imprint. Voids and micro-cracks (indicated by arrows) evidence the initial corrosion attach to the substrate.

The minor consequences of the Vickers test are visualized by the pictures in Fig. 14.

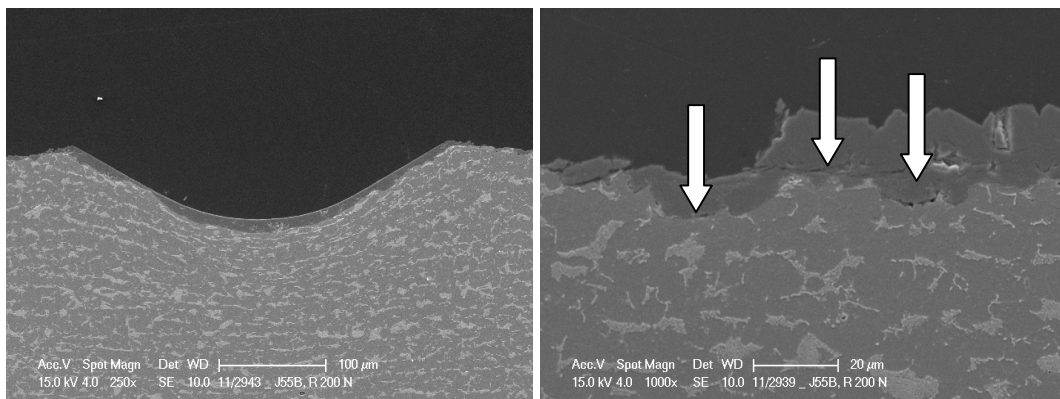


Figure 13: SEM micrograph (SE) of the cross section of the corroded J55 steel sample after Rockwell indentation at 200 N maximum load: side B in contact with the autoclave bottom (Markers: 100 μm on the left, 20 μm on the left).

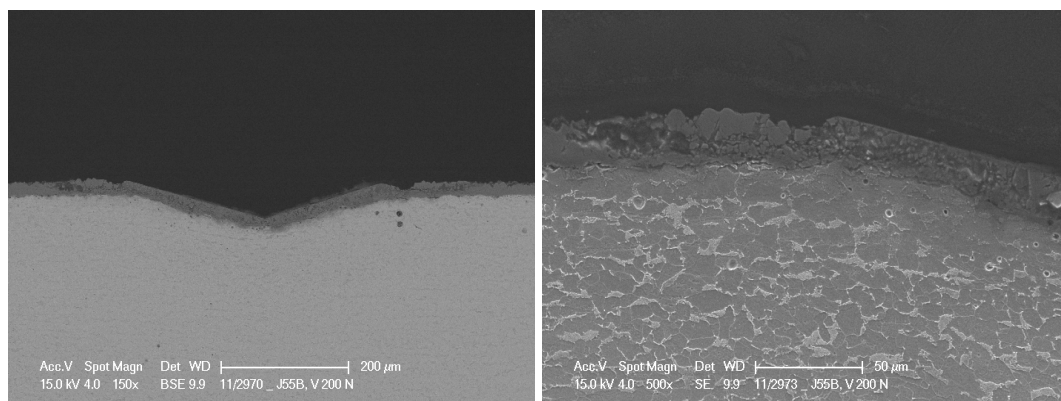


Figure 14: SEM micrograph (SE) of the cross section of the corroded J55 steel sample after Vickers indentation at 200 N maximum load: side B in contact with the autoclave bottom (Markers: 200 μm on the left, 50 μm on the left).

CLOSING REMARKS

Corrosion layers grown on two different pipe steel substrates in a common controlled environment were subjected to indentation tests carried out at different maximum load and with different tip geometry. The results of this preliminary investigation evidence the following features:

- (i) indentation represents a rather effective characterization tool that permits to identify single and/or double corrosion layers forming on the steel, the main mechanical characteristics and the spalling attitude;
- (ii) brittleness induced in double corrosion layers is reflected by kinks in the otherwise smooth indentation curves;
- (iii) cracks appearing in the region underneath the wide areas of removed crystals in double corrosion layers are evidenced by SEM investigations;
- (iv) the steel substrate plays a role in enhancing or reducing the adhesion properties of the scales;
- (v) contrary to different quasi-brittle material systems, which are more sensitive to sharp indenters [19], the effect of damage phenomena on indentation curves is magnified by the axis-symmetric Rockwell tip.

ACKNOWLEDGEMENT

The assistance provided at Venezia Tecnologie S.p.A. by Dr. Sergio Sgorlon for sample preparation and by Dr. M. Battagliarin for micrographic studies, and at the Politecnico di Milano by Eng. Marco Talassi for the indentation tests is gratefully acknowledged.

REFERENCES

- [1] Baker, M.Jr, Fessler, R.R., Pipeline corrosion, Report submitted to the US Department of Transportation, Pipeline and Hazardous Materials Safety Administration, Office of Pipeline Safety, (2008).
- [2] Bolzon, G., Boukharouba, T., Gabetta, G., Elboujdaini, M., Mellas, M. (Eds.), Corrosion Protection of Pipelines Transporting Hydrocarbons, NATO Science for Peace and Security Series C: Environmental Security, Springer, Dordrecht, (2011).
- [3] API 5L Specification for line pipe, American Petroleum Institute, Washington DC, (2004).
- [4] Palacios, C.A., Shadley, J.R., Characteristics of corrosion scales on steels in a CO₂-saturated NaCl brine, *Corrosion*, 47 (1991) 122–127.
- [5] Gao, K., Yu, F., Pang, X., Zhang, G., Qiao, L., Chu, W., Lu, M., Mechanical properties of CO₂ corrosion product scales and their relationship to corrosion rates, *Corrosion Sci.*, 50 (2008) 2796–2803.
- [6] Zhang, Y., Pang, X., Qu, S., Li, X., Gao, K., The relationship between fracture toughness of CO₂ corrosion scale and corrosion rate of X65 pipeline steel under supercritical CO₂ condition, *Int. J. Greenhouse Gas Control*, 5 (2011) 1643–1650.



- [7] ISO 6508–1:2005, Metallic materials – Rockwell hardness test – Part 1: Test method (scales A, B, C, D, E, F, G, H, K, N, T), International Organization for Standardization, Geneva, (2005).
- [8] ISO 6507–1:2005, Metallic materials – Vickers hardness test – Part 1: Test method, International Organization for Standardization, Geneva, (2005).
- [9] Bolzon, G., Bocciarelli, M., Chiarullo, E.J., Mechanical characterization of materials by micro-indentation and AFM scanning, in: Applied scanning probe methods XII – Characterization, B. Bhushan and H. Fuchs (Eds.), Springer, Berlin (2008) 85–120.
- [10] Bolzon, G., Molinas, B., Talassi, M., Mechanical characterization of metals by indentation tests: an experimental verification study for on site applications, *Strain*, 48 (2012) 517–527.
- [11] Bolzon, G., Gabetta, G., Molinas, B., Safety assessment of pipeline systems by an enhanced indentation technique, *J. Pipeline Syst. Eng. Pract.* (2014).
- [12] Nykyforchyn, H., Lunarska, E., Tsyurulnyk, O.T., Nikiforov, K., Gennaro, M.E., Gabetta, G., Environmentally assisted “in-bulk” steel degradation of long term service gas trunkline, *Eng. Fail. Anal.*, 17 (2010) 624–632.
- [13] Bocciarelli, M., Bolzon, G., Indentation and imprint mapping for the identification of constitutive parameters of thin layers on substrate: Perfectly bonded interfaces, *Mat. Sci. Eng. A*, 448 (2007) 303–314.
- [14] Bocciarelli, M., Bolzon, G., Indentation and imprint mapping for the identification of interface properties in film-substrate systems, *Int. J. Fract.*, 155 (2006) 1–17.
- [15] Bhushan, B., Li, X., Nanomechanical characterisation of solid surfaces and thin films, *Int. Mat. Rev.*, 48 (2003) 125–164.
- [16] API 5CT Specification for casing and tubing, American Petroleum Institute, Washington DC, (2011).
- [17] Molinas, B., Battagliarin, M., Sgorlon, S., Gennaro, M.E., Nesic, S., Yang, Y., Gabetta, G., Proprietà meccaniche e meccanismi di frattura in “scales”-modello di carbonati di ferro, in: AIM, Giornate nazionali sulla Corrosione e Protezione, IX edizione, Monte Porzio Catone (Roma), Italy, (2011).
- [18] Gabetta, G., Balostro, V., Bolzon, G., Battagliarin, M., Molinas, B., Mechanical properties of iron-based scales in CO₂ corrosion modeling, in: NACE Corrosion 2012, Research in Progress Symposium, Salt Lake City, USA, (2012).
- [19] Bolzon, G., Chiarullo, E.J., Egizabal, P., Estournes, C., Constitutive modelling and mechanical characterization of aluminium-based metal matrix composites produced by spark plasma sintering, *Mech. Mat.*, 42 (2010) 548–558.